New Journal of Physics
The open access journal at the forefront of physics

Deutsche Physikalische Gesellschaft DPG IOP Institute of Physics

Negative differential conductance in the electron-transport through copper-rich cuprous oxide thin films

New Journal of Physics
The open access journal at the forefront of physics

Deutsche Physikalische Gesellschaft DPG
IOP Institute of Physics

Published in partnership with: Deutsche Physikalische Gesellschaft and the Institute of Physics

OPEN ACCESS

RECEIVED
19 July 2019

REVISED
6 October 2019

ACCEPTED FOR PUBLICATION
28 October 2019

PUBLISHED
13 November 2019

PAPER

Negative differential conductance in the electron-transport through copper-rich cuprous oxide thin films

Alexander Gloystein, Christoph Möller and Niklas Nilius

Institut für Physik, Carl von Ossietzky Universität, Oldenburg, Germany

E-mail: niklas.nlius@uni-oldenburg.de

Keywords: electron transport, negative differential conductance, p-type oxides, metal nanoparticles, quantisation

Supplementary material for this article is available online

Abstract

Copper deposition onto Cu_2O thin films grown on Au(111) results in the formation of monolayer islands with hexagonal and rhombic shapes, as observed with scanning tunnelling microscopy. The differential conductance through the Cu islands is governed by distinct quantum well states (QWS), accompanied by pronounced electron standing wave patterns. Below the onset of the QWS, an extended region of negative differential conductance opens up, in which also the tunnelling current declines markedly with increasing bias voltage. The effect is assigned to the quantised electronic structure of the Cu islands in combination with the p-type conductance behaviour of the oxide film underneath. The latter promotes electron transport across the islands around the Fermi level, but leads to a closure of this transport channel at negative bias.

1. Introduction

A fundamental goal in the development of novel electronic devices is the fabrication of elements with strongly nonlinear current–voltage characteristics [1]. Such a conductance behaviour beyond Ohms law forms the basis for various electronic applications, e.g. switches, amplifiers and smart control systems. Of particular interest are elements with negative differential resistance (NDR), exhibiting a decreasing current at increasing voltage or synonymously a differential conductance (dI/dV) with negative sign. On the mechanistic level, the NDR effect typically arises from electron tunnelling through systems with a strongly non-monotonic density of states (DOS) [2]. The technologically most relevant example is the tunnelling diode, made of highly p- and n-doped electrodes facing each other across an insulating gap. Electron tunnelling across the gap gives rise to the NDR effect with ratios between forward and valley current of about ten.

The NDR effect has been identified in a large variety of quantum systems. It is commonly found in the electron transport through individual molecules and molecular films [3–6], and arises if a conductance channel through a molecular orbital becomes non-resonant with the leads of the junction [7, 8]. Alternatively, the NDR effect may be triggered by conformational changes in the molecules, which modify the transparency of the molecular DOS for electrons [9]. However, negative differential conductance is not restricted to molecular systems and has been found in inorganic materials as well, provided they feature discrete energy levels suitable for electron transport [10]. It has been observed, for example, in the tunnelling characteristic of Cl vacancies in NaCl thin films or of band-gap states in boron- or hydrogen-terminated Si(111) [11–13]. Also the conductance through Gd nanowires self-assembled on Si(110) displays a pronounced NDR region at negative bias [14]. In all these examples, conductance spectroscopy with a scanning tunnelling microscope (STM) was the method of choice to probe the NDR effect. The technique features unmatched spatial resolution and is thus sensitive to individual nanostructures. Moreover, it enables an easy adjustment of the Fermi levels (E_F) of the involved electrodes in order to realise resonant tunnelling conditions.

Also metal particles with a few hundreds or thousands of atoms are characterised by a discrete DOS, which in principle qualifies them for the NDR effect. The latter should be particularly strong in 2D islands, where quantisation phenomena are more pronounced than in 3D systems [15]. Moreover, metal nanostructures are

expected to be more robust against damage at high current loads as compared to molecules. Despite these advantages, NDR effects have rarely been reported in the electron transport through metal nanostructures, mostly for two reasons [16]. First, metal particles are often prepared on dielectric supports with low surface-free energy, where Vollmer–Weber growth guarantees the formation of compact and spatially confined aggregates [17]. Given the low conductivity of most dielectrics, electron-transport in these samples is often governed by Coulomb charging instead of NDR effects [18, 19]. Second, quantum well states (QWS) in nanoparticles are often closely-spaced and strongly overlapping, which makes NDR-related phenomena difficult to observe [20].

In this work, a compound system made of a cuprous oxide thin film decorated with monolayer (ML) Cu islands is presented, in which the above two restrictions are lifted and a strong NDR effect becomes visible in STM spectroscopy. Electron transport through the contact is governed by the QWS of the Cu flakes in combination with the p-type conductance behaviour of the Cu_2O layer beneath. The interplay of both contributions leads to an extended NDR region just below the onset of the copper QWS at negative bias, characterised by a large ratio between on/off current.

2. Experimental techniques

The experiments have been performed with a custom-built Beetle-type STM, operated at liquid nitrogen temperature. The microscope is enclosed in an UHV chamber (base-pressure 2×10^{-10} mbar), equipped with standard facilities for sample preparation and analysis. The STM measurements were conducted in the constant current mode with electrochemically etched gold tips. Differential conductance data were recorded with a lock-in amplifier at 15 mV modulation bias and 1350 Hz. The oxide films were prepared by reactive Cu deposition onto a sputtered and annealed Au(111) single crystal in 5×10^{-6} mbar oxygen ambience [21]. To stimulate crystallisation, the films were post-annealed in vacuum to 600 K until a sharp (2×2) spot pattern with respect to the primitive Au (1×1) was detected in electron diffraction. The film thickness after annealing was estimated to four MLs. The films have Cu_2O stoichiometry and feature a 2.0 eV band gap, as probed with STM conductance spectroscopy. In addition, a surface state is revealed in the unoccupied part of the band gap, arising from the Cu 4*s* dangling bond state of chemically unsaturated Cu_{cus} ions according to recent density functional theory calculations [22]. Tunnelling into this resonance produces a hexagonal lattice with 5.8 Å periodicity in the STM, characteristic for the $Cu_2O(111)$ surface (figure 1(a)). The oxide film is permeated by dislocation lines, compensating for the misfit strain with the gold support. Depending on thickness and thermal treatment of the Cu_2O layer, the domain boundaries adopt triangular, zig-zag and straight configurations [23]. The films prepared here are composed of triangular domains with 5 nm edge length. The sample preparation was finalised by dosing 0.2 ML of metallic Cu onto the oxide surface followed by an annealing step to temperatures between 400 and 600 K.

3. Experimental results

Figure 1(a) depicts a large-scale STM topography of Cu_2O/Au(111), clearly displaying the hexagonal atomic lattice and the triangular domain pattern of the film. After copper deposition at 300 K, the oxide surface gets decorated with small particles without discernible inner structure (figure 1(a), inset). Gently annealing to 450 K triggers a rearrangement of the ad-copper into ML islands of hexagonal or rhombic shape and ~5 nm edge length (figure 1(b)). Two island configurations are distinguishable, ad-islands that protrude the oxide by 1.0 Å and embedded island being 1.5 Å lower than the oxide surface (figure 1(d)). These height values have been recorded at 2.5 V sample bias and exhibit a strong bias dependence indicative for an electronic contribution. The island boundaries perfectly follow the symmetry directions of the Cu_2O lattice, suggesting a template effect of the oxide surface. Rough boundaries were only observed in vicinity of Cu_2O step edges most likely due to a deviating nucleation mechanism. No inner structure was resolved for the Cu islands, however, the spectroscopy data presented later suggest a dense-packed Cu(111) nature. Further annealing to 600 K leads to a substantial increase of the island diameter to 10–20 nm, a clear sign for Ostwald ripening at elevated temperature (figure 1(c)). Although the structural integrity of the underlying Cu_2O cannot be proven from the topographic data, our conductance spectra suggest the presence of an oxide spacer even after annealing. Rising the temperature to 700 K finally destroys the oxide film and renders the pristine Au(111) surface visible in the STM. The oxide decomposition is driven by Cu dissolution into the Au support, associated with oxygen desorption from the surface [23]. The peculiar electronic structure of ML Cu islands on Cu_2O/Au(111) is addressed in the following paragraph.

Differential conductance (dI/dV) spectra taken on pristine Cu_2O films feature a wide region of low intensity, reflecting the Cu_2O band gap around the Fermi level (figure 2(a), second curve). An in-gap peak at 0.85 V marks the dangling-bond state of Cu_{Cus} surface ions discussed before [22]. The dI/dV response changes

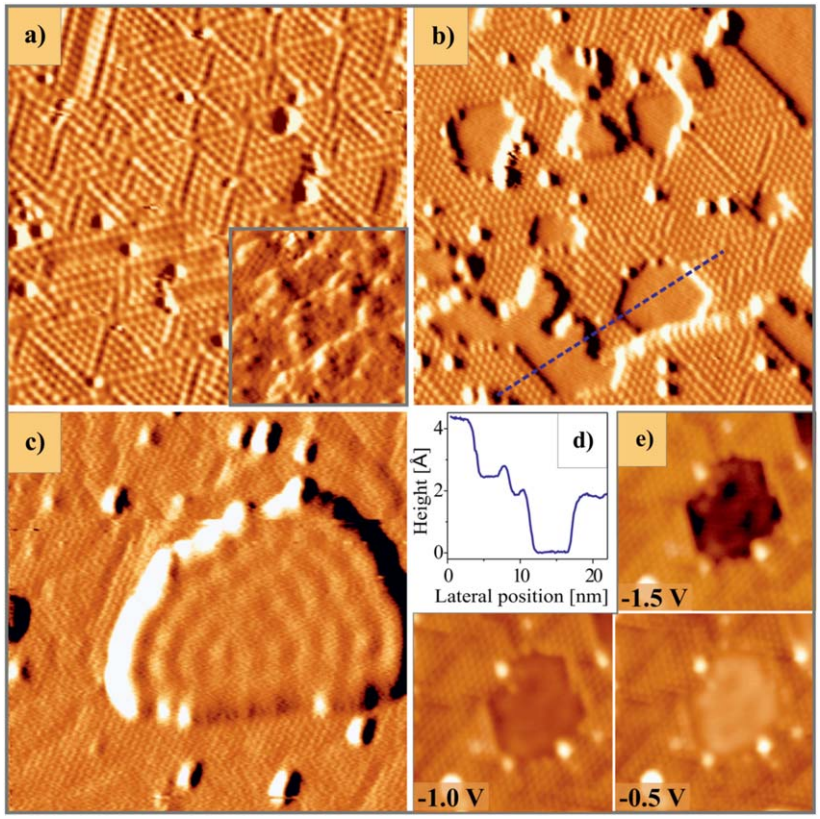

Figure 1. STM topographic images of (a) pristine Cu_2O/Au(111), (b) after deposition of 0.2 ML Cu and 450 K annealing and (c) after 600 K annealing (30 × 30 nm^2, U_B = 2.2 V, 10 pA). The inset in (a) shows the surface after 0.2 ML Cu deposition prior to annealing (30 × 30 nm^2). (d) Height profile corresponding to the dashed line in panel (b). (e) Bias-dependent STM images of a Cu island depicting a contrast reversal between −1.0 and −0.5 V sample bias (15 × 15 nm^2).

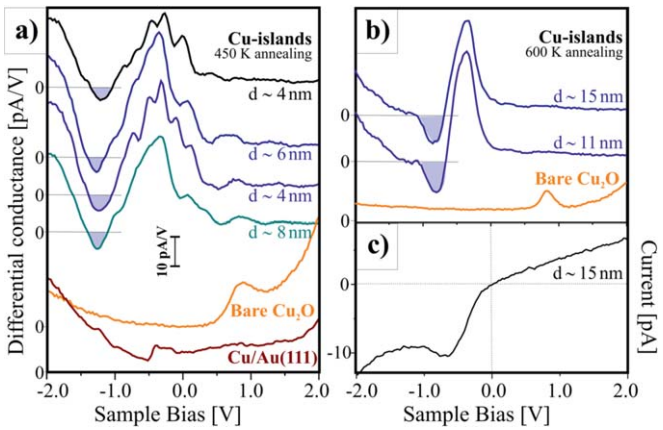

Figure 2. (a) Differential conductance spectra measured on oxide-free Cu/Au(111), a bare Cu_2O film and Cu ad-islands produced by 450 K sample annealing (bottom to top). (b) Similar data as in (a) but after 600 K annealing. (c) Current trace measured simultaneously with the upper dI/dV curve in (b). The mean size of examined Cu islands is indicated in the panels, the NDR regions are marked with blue areas. All spectroscopy data were taken at a set point of 2.0 V and 10 pA. See supplementary material for spectra measured as a function of set-point current.

drastically when moving the tip on top of the Cu ad-islands, both the adsorbed and embedded type (figure 2(a), upper curves). While the conductance above E_F is featureless and lacks the oxide surface state seen before, a series of pronounced dI/dV maxima becomes visible at negative bias. The maximum dI/dV intensity is typically reached at −0.3 V, below which the conductance starts decreasing again. Surprisingly, the dI/dV signal turns negative in a broad bias window around −1.0 V and only slowly recovers to positive values at even higher negative bias. The effect is particularly strong for the largest ad-islands produced by 600 K annealing, where the ratio between maximum and valley conductance (on/off) amounts to 3:1 (figure 2(b)). As a result, the NDR

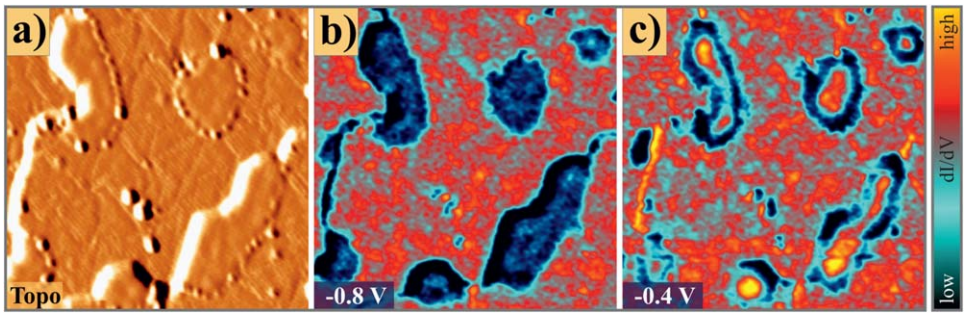

Figure 3. STM topographic image and corresponding dI/dV maps of Cu islands on Cu_2O/Au(111) (50 × 50 nm^2, −0.8 V, 10 pA). The ad-islands are clearly distinguishable via their distinct conductance behaviour. They appear dark in the NDR region at −0.8 V and develop bright centres at −0.4 V due to tunnelling from the copper QWS.

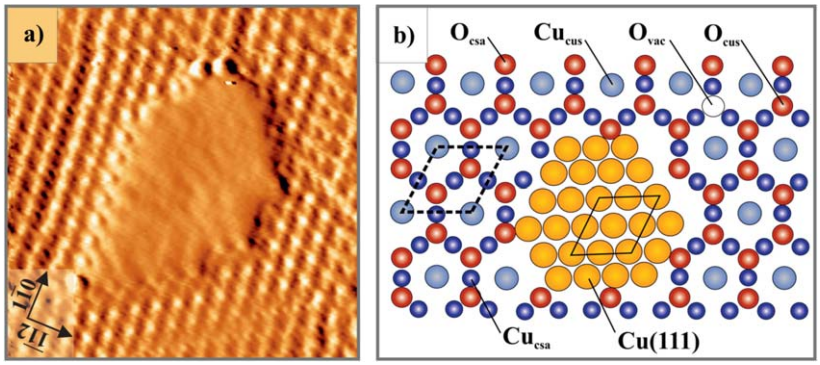

Figure 4. High resolution STM image and proposed growth model of Cu islands embedded in the surface of a Cu_2O/Au(111) thin film (10 × 10 nm^2, U_B = 0.5 V, 10 pA).

effect is not only detected in the dI/dV spectra but appears directly in the I–V curves (figure 2(c)). We note that the phenomenon is neither observed for Cu islands grown directly on Au(111) (figure 2(a), lowest curve) nor for islands bound to ML-thick oxide films.

The high conductance at and below E_F makes the Cu ad-islands easily detectable in dI/dV maps, even if the topographic contrast to surrounding Cu_2O patches is small (figure 3). In maps taken just below E_F, the copper islands appear brighter than the surrounding oxide, an effect that reverses in the NDR region at around −1.0 V. The nature of the unusual conductance signature of ML Cu islands on Cu_2O thin films is discussed in the next section.

4. Discussion

Cu_2O(111), a close-packed oxide surface with comparatively low surface-free energy, is expected to promote Vollmer–Weber growth of metals, resulting in compact 3D particles [24, 25]. However, not even room-temperature Cu exposure gives rise to discernible 3D deposits, and the deviation from Vollmer–Weber growth becomes striking after annealing the Cu/Cu_2O system. Already at 450 K, the ad-copper aggregates to perfect ML islands, embedded either in the surface plane or in deeper oxide layers. The protruding appearance of the ad-islands at certain bias voltages only reflects the higher DOS of the metal with respect to the oxide and is therefore an electronic and not a topographic effect (see figure 1(e)). The unusual growth behaviour of copper on Cu_2O/Au(111) is ascribed to the low thermodynamic stability of the oxide film, especially in Cu excess. Already at moderate vacuum-annealing, the low-coordinated O_{Cus} ions start desorbing from the surface and the emerging voids fill up with Cu ad-atoms from the evaporation process. The latter merge with neighbouring Cu^+ ions from the oxide network and aggregate to metallic Cu flakes with a Cu(111)-type packing (figure 4). At even more reducing conditions, also O ions from subsurface Cu_2O planes may leave the lattice, allowing the Cu islands to etch deeper into the Cu_2O film and to form the embedded island type.

The well-established electronic properties of compact Cu(111) planes provide a good starting point for discussing the conductance phenomena observed for the oxide-supported islands. Their DOS around E_F is

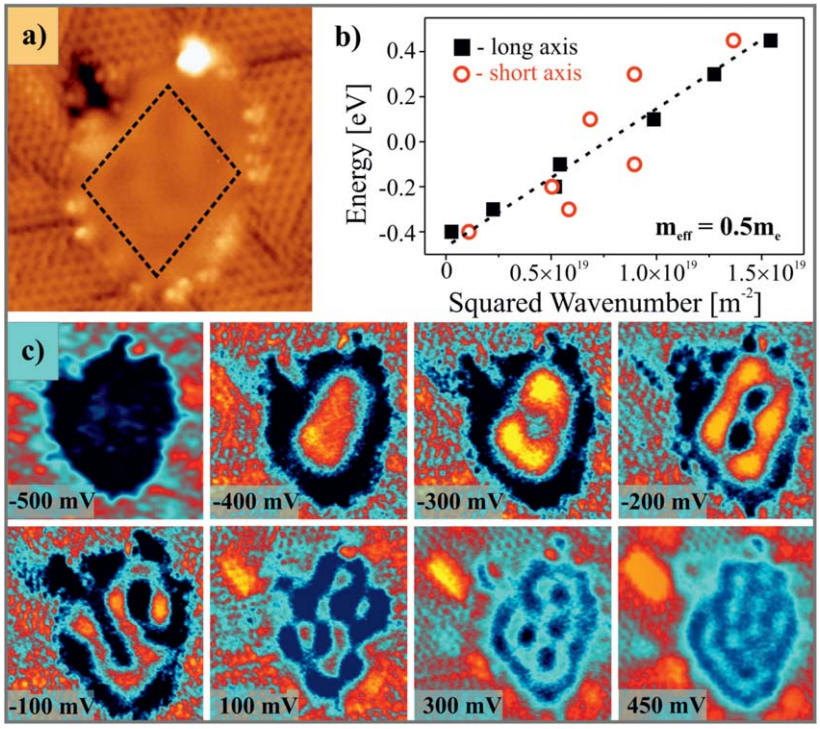

Figure 5. (a) STM topography and (c) associated dI/dV maps for a rhombic Cu ad-island on Cu_2O/Au(111) taken at the indicated bias voltages (12.5 × 12.5 nm^2). (b) Dispersion relation of the derived electronic states and fit to an E~k^2 free-electron model. The graph does not include the effects of bias-division.

dominated by the Cu 4*sp* band that can be approximated as free-electron parabola near the band onset [26]. On infinite Cu(111), the band takes the form of a Shockley surface state with −450 meV energy onset and 0.46m_e effective electron mass [27]. Deviations from the ideal free-electron parabola are expected here due to the finite size and ML character of the ad-islands. The filled Cu 3*d* states, on the other hand, are located at energies below −2.0 eV and not relevant for the observed conductance behaviour.

The measured dI/dV spectra of Cu ad-islands can indeed be rationalised with the signature of a quantised Cu 4*sp* surface band. The sudden conductance rise at about −0.7 V agrees reasonably well with the band onset [27]. Deviations from the classical surface state arise from the peculiar tunnelling characteristic through a double-barrier junction that consists of vacuum gap, Cu island and Cu_2O film in the present case. Due to a finite screening ability, a part of the applied bias drops inside the oxide layer and not in the vacuum barrier, which results in a systematic shift of measured onset positions to more negative values [28, 29]. The ratio between bias-drop in the oxide film and the vacuum gap amounts to: $\eta = \frac{d}{\varepsilon z}$ with d and $\varepsilon = 7.1$ being the thickness and dielectric constant of the Cu_2O film and z the tip-sample distance [30]. Using approximate values for film thickness (4 ML) and tunnelling distance (6.5 Å at 2 V bias setpoint, see supplementary material available online at stacks.iop.org/NJP/21/113026/mmedia), η is calculated to 0.2 and all spectral features appear at $\eta/(\eta + 1) = 17\%$ higher voltage than in the unbiased junction. This bias division partly explains, why measured band onsets in the oxide-supported Cu islands are systematically shifted with respect to the classical Cu(111) Shockley band [31].

Above the band onset, the dI/dV spectra run through a series of maxima, whereas the ideal Shockley band features constant DOS (figure 2(a)). This observation provides evidence for electron quantisation in the Cu islands that are smaller than the Fermi wavelength of copper [32, 33]. Only in the largest flakes produced by 600 K annealing, the spacing between adjacent QWS becomes too small to induce a discernible fine-structure in the dI/dV spectra (figure 2(b)). Electron quantisation comes along with pronounced standing-wave patterns in the respective dI/dV maps [15, 34], exemplarily shown for a nearly rhombic Cu island in figure 5. Below the band onset, i.e. in the NDR region, the island exhibits dark dI/dV contrast. Increasing the bias to −0.4 V moves the lowest QWS into the focus and an elongated conductance maximum emerges in the island centre. At −0.3 V, the second QWS becomes detectable as dumbbell pattern with a single node along the long island axis. The following state, characterised by two orthogonal nodal planes, appears at −0.2 V, while development of a second node along the long axis is observed at −0.1 V. Additional QWS are detected above E_F, however, more and more complex wave patterns render their assignment to specific eigenstates difficult.

From analysing energy and nodal structure of the detected QWS, the onset and dispersion of the Cu 4*sp* band can be determined. The experimental island in figure 5 does not have a simple spherical or hexagonal symmetry, but can be approximated with a distorted rectangle of 6.9 × 5.7 nm edge lengths. The dispersion along the two separable axes is then given by: $E_{x,y} = E_0 + \frac{\hbar^2}{2m_{\mathrm{eff}}} k_{x,y}^2$ with m_{eff} the effective electron mass [35]. The wavenumber $k_{x,y} = \frac{2\pi}{\lambda_{x,y}}$ can be extracted from intrinsic wavelengths of the QWS maxima, as derived from fitting cross sections along the island axes to a squared sine function. The resulting graph depicts the expected $E{\sim}k^2$ dependency of a quasi-free electron gas in a box potential. A linear fit to data from both axes yields a band onset of $E_0 = -(500 \pm 60)$ meV and an effective electron mass of $m_{\mathrm{eff}} = (0.5 \pm 0.1)\, m_{\mathrm{e}}$. After correcting for the bias-division in the double barrier junction, the band onset agrees with the one of the Cu(111) surface state, while the effective mass is somewhat larger ($0.65 m_{\mathrm{e}}$ instead of $0.46 m_{\mathrm{e}}$). Higher effective mass indicates larger interatomic distances, hence reduced wavefunction overlap in the ad-islands, which might be explained with a template effect of the spatially expanded Cu_2O(111) surface [36]. We note that different ad-islands feature different dispersion relations. The QWS in hexagonal islands, as seen in figure 1(b) for example, show a nearly linear dispersion due to wavefunction entanglement along the island axes. A more detailed discussion of quantisation phenomena in the differently shaped ad-islands on Cu_2O(111) is however beyond the scope of this paper.

Our analysis indicates that the conductance behaviour of the Cu islands can be understood from the properties of the Cu *4sp* surface band modified by electron quantisation effects. However, deviations are evident at two points. The first one is the detected dI/dV signal strength, being much higher for filled than for empty QWS. In fact, the empty QWS at positive bias are hardly resolved at all (figure 2). This discrepancy cannot be explained with deviating matrix elements for the tunnelling process, as tunnelling into empty states is typically easier than from filled states due to a higher spatial confinement of the latter. The second point concerns the anomalous conductance course with an extended NDR region below the Cu 4*sp* band. While a drop of the dI/dV signal always occurs at the band onset, as no new transport channels become available anymore, the signal should remain above zero. The pronounced NDR effect observed here suggests an additional effect, which may be connected to the p-type conductance behaviour of the Cu_2O thin films, as sketched in our final section.

A current flow through the Cu ad-islands requires both, vacuum tunnelling into/out of the STM tip and electron transport across the Cu_2O film, being a bulk insulator with 2.15 eV band gap [37]. In stoichiometric Cu_2O with the Fermi level in mid-gap position, this extra barrier affects the dI/dV spectra in similar manner for both polarities. The symmetry gets lifted if the balance of charge carriers gets perturbed and the Fermi level shifts towards one band edge. Cuprous oxide is a textbook example for a p-type conductor, as formation of Cu vacancies is thermodynamically preferred [38]. Development of a p-type Cu_2O film is expected also in our case, although metallic copper, formally an electron donor, is dosed onto the surface. This apparent contradiction may be resolved as follows. Formation of Cu ad-islands is always initiated by a vacuum-annealing step, stimulating oxygen desorption from the surface. The voids are populated by deposited Cu atoms that merge with adjacent Cu ions of the film to a compact island, as visualised in figure 4. Each desorbing O species hereby releases two electrons, formally enough to neutralise two adjacent Cu^+ ions. If more than two cations are involved in the process, for example if all Cu^+ neighbours of an oxygen vacancy turn metallic, the missing charges are pulled off the surrounding Cu_2O network that consequently turns electron-deficient. The spread of metallic Cu islands in the Cu_2O surface might therefore result in a p-type conductance behaviour of the oxide film (figure 4).

The mechanism of electron transport through a Cu / p-type Cu_2O / Au(111) tunnel junction is now discussed separately for the different voltage regimes depicted in figure 6. At positive sample bias, electron propagation from the tip to the sample can be realised in a single step, in which the electron tunnels through vacuum barrier, Cu island and Cu_2O band gap into an accepting state of the Au(111) surface. In the case of a finite residence time of electrons in the Cu eigenstates, the one-step process would be replaced by a two-step tunnelling scheme and the signature of Coulomb charging should appear in the conductance traces. However, experimental dI/dV spectra are nearly featureless at positive bias and no signs of sequential tunnelling are revealed. A one-step tunnelling regime also explains the low dI/dV intensities measured above E_{F}, because the total tunnelling distance, consisting of vacuum plus oxide barrier, is relatively long (figure 6(a)).

The situation changes at small negative bias, where two steps are mandatory to propagate electrons from the Au(111) to the tip (figure 6(b)). In a first step, tunnelling occurs from occupied QWS in the Cu island to empty tip states. Corresponding rates are expected to be large, given the much shorter tunnelling distance with respect to the one-step process discussed before. In a second step, the electron reservoir in the Cu islands is refilled by moving the hole through the oxide spacer into the gold support. Also this process is associated with high rates for the following reasons: (i) At low bias, the hole in the copper QWS safely faces the valence band of the p-type Cu_2O, even if it thermalizes to the islands Fermi level. (ii) Hole transfer into and out of the oxide bands occurs without hindrance, as the Cu_2O films are too thin to develop Schottky barriers either on the gold or the copper side. (iii) Hole transport inside the oxide film is governed by the excellent hole-conducting properties of cuprous

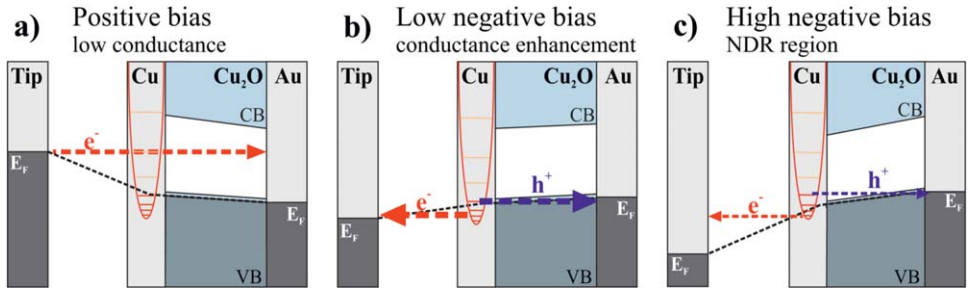

Figure 6. Electron-transport through a $Cu/Cu_2O/Au(111)$ tunnel junction at (a) positive, (b) small negative and (c) large negative bias. The limiting step is the hole transport from the Cu QWS into the Cu_2O valence band.

oxide [37], and further promoted by an only partly screened tip-electric field. And (iv), quick refilling of the copper QWS is guaranteed as the entire island area and not only the position of the tip is available for charge exchange. In total, electron transport between sample and tip is highly efficient at small negative bias, explaining the large dI/dV signal observed in the region of filled copper QWS.

However, this conductance channel breaks down at higher negative bias and leads to the extended NDR region below the onset of the Cu *4sp* band (figure 6(c)). While the first transport step that is electron tunnelling from filled QWS states to the tip remains open, the hole transport through the oxide layer gets disrupted. The reason is a tip-induced downward bending of the Cu_2O valence band, which in turn does not face the hole-state in the copper QWS anymore. Especially if the hole thermalizes to the Fermi level, penetration into the p-conductive Cu_2O film is blocked by a tunnel barrier and the hole gets trapped at the top of the filled QWS. As a consequence, electron transport through the STM junction gets inhibited, which results in a sudden drop of the tunnelling current and drives the system into the NDR regime (figure 6(c)). The same explanation holds when switching the view point from hole to electron transport. Also here, charge transfer from Au(111) to the copper QWS is the decisive step. Whereas at low negative bias, it relies on direct conductance through a partially filled Cu_2O valence band, it involves tunnelling across the Cu_2O band gap as the bias increases. The proposed mechanism deviates from common NDR concepts, in which a discrete electronic state, e.g. a molecular orbital, turns non-resonant with the Fermi energy in either tip or sample [2–6]. Indirect support for our interpretation comes from the fact that no comparable conductance behaviour has been observed for the various particle-oxide systems explored with STM so far [39]. Most of these experiments were performed on stoichiometric or n-type oxide films that are either unable to modify electron transport at all or promote conductance through empty QWS.

5. Conclusions

ML Cu islands grown on Cu_2O thin films are subject to lateral quantisation effects that come along with pronounced electron standing wave patterns, as detected with scanning tunnelling microscopy and spectroscopy. Especially the filled Cu 4*sp*-derived QWS give rise to a series of pronounced dI/dV maxima, while empty QWS are hardly detected in the spectra. The effect was explained with the p-type conductance behaviour of the oxide film directly below the Cu islands. While at positive bias, the oxide band gap poses a barrier for electron tunnelling, the transport gets promoted by the high-lying valence band of p-type Cu_2O at small negative bias. At high negative bias, on the other hand, this conductance channel breaks down and a wide NDR region opens up below the copper QWS states. The NDR effect thus arises from the interplay of electron quantisation, a p-type conductance behaviour and the dielectric screening in the $Cu/Cu_2O/Au(111)$ tunnel junction. Future studies aim at optimising the NDR effect by tuning layer thickness, defect structure and p-type character of the Cu_2O films.

Acknowledgments

We thank Claudine Noguera and Jacek Goniakowski for many insightful discussions. Financial support is acknowledged from the DFG Grant Ni 650-4 ‘Properties of pristine and doped copper oxide thin films’.

ORCID iDs

Niklas Nilius https://orcid.org/0000-0003-0264-120X

References

[1] Papadopoulos C 2014 *Solid-State Electronic Devices* (New York: Springer)
[2] Agrait N, Yeyati A L and van Ruitenbeek J M 2003 *Phys. Rep.* **377** 81
[3] Grobis M, Wachowiak A, Yamachika R and Crommie M F 2005 *Appl. Phys. Lett.* **86** 204102
[4] Tu X W, Mikaelian G and Ho W 2008 *Phys. Rev. Lett.* **100** 126807
[5] Heinrich B W, Rastei M V, Choi D J, Frederiksen T and Limot L 2011 *Phys. Rev. Lett.* **107** 246801
[6] Xu B and Dubi Y 2015 *J. Phys.: Condens. Matter* **27** 263202
[7] Guisinger N P, Greene M E, Basu R, Baluch A S and Hersam M C 2004 *Nano Lett.* **4** 55
[8] Chen F, Hihath J, Huang Z F, Li X L and Tao N J 2007 *Annu. Rev. Phys. Chem.* **58** 535
[9] Gaudioso J, Lauhon L J and Ho W 2000 *Phys. Rev. Lett.* **85** 1918
[10] Wang S, Lu W, Zhao Q and Bernholc J 2006 *Phys. Rev.* B **74** 195430
[11] Repp J, Meyer G, Paavilainen S, Olsson F E and Persson M 2005 *Phys. Rev. Lett.* **95** 225503
[12] Berthe M, Stiufiuc R, Grandidier B, Deresmes D, Delerue C and Stiévenard D 2008 *Science* **319** 436
[13] Rashidi M, Taucer M, Ozfidan I, Lloyd E, Koleini M, Labidi H, Pitters J L, Maciejko J and Wolkow R A 2016 *Phys. Rev. Lett.* **117** 276805
[14] Hong I H, Chen T M and Tsai Y F 2012 *Appl. Phys. Lett.* **101** 053113
[15] Lin X, Nilius N, Freund H-J, Walter M, Frondelius P, Honkala K and Häkkinen H 2009 *Phys. Rev. Lett.* **102** 206801
[16] Zhang H, Mautes D and Hartmann U 2007 *Nanotechnology* **18** 6
[17] Freund H-J 2002 *Surf. Sci.* **500** 271
[18] Hanna A E and Tinkham M 1991 *Phys. Rev.* B **44** 5919
[19] Nilius N, Kulawik M, Rust H-P and Freund H-J 2004 *Surf. Sci.* **572** 347
[20] Kuemmeth F, Bolotin K I, Shi S F and Ralph D C 2008 *Nano Lett.* **8** 4506
[21] Sträter H, Fedderwitz H, Groß B and Nilius N 2015 *J. Phys. Chem.* C **119** 5975
[22] Nilius N, Fedderwitz H, Groß B, Noguera C and Goniakowski J 2016 *Phys. Chem. Chem. Phys.* **18** 6729
[23] Möller C, Fedderwitz H, Noguera C, Goniakowski J and Nilius N 2018 *Phys. Chem. Chem. Phys.* **20** 5636
[24] Campbell C T 1997 *Surf. Sci. Rep.* **27** 1
[25] Soon A, Todorova M, Delley B and Stampfl C 2007 *Phys. Rev.* B **75** 125420
[26] Courths R, Lau M, Scheunemann T, Gollisch H and Feder R 2001 *Phys. Rev.* B **63** 195110
[27] Kevan S D and Gaylord R H 1987 *Phys. Rev.* B **36** 5809
[28] Feenstra R M 1994 *Phys. Rev.* B **50** 4561
[29] de Raad G J, Bruls D M, Koenraad P M and Wolter J H 2002 *Phys. Rev.* B **66** 195306
[30] Wu S W, Nazin G V, Chen X, Qui X H and Ho W 2004 *Phys. Rev. Lett.* **93** 236802
[31] Cui Y, Stiehler C, Nilius N and Freund H-J 2015 *Phys. Rev.* B **92** 075444
[32] Lagoute J, Liu X and Fölsch S 2005 *Phys. Rev. Lett.* **95** 136801
[33] Stiehler C, Pan Y, Schneider W-D, Koskinen P, Häkkinen H, Nilius N and Freund H-J 2013 *Phys. Rev.* B **88** 115415
[34] Kliewer J, Berndt R and Crampin S 2001 *New J. Phys.* **3** 22
[35] Kittel C 1996 *Introduction to Solid State Physics* (New York: Wiley)
[36] Schmid G 2004 *Nanoparticles: from theory to application* (Weinheim: Wiley-VCH)
[37] Meyer B K *et al* 2012 *Phys. Status Solidi* b **249** 1487
[38] Raebiger H, Lany S and Zunger A 2007 *Phys. Rev.* B **76** 045209
[39] Nilius N 2009 *Surf. Sci. Rep.* **64** 595